Mineralogy and Reactive Fluid Chemistry Evolution of Hydraulically Fractured Caney Shale of Southern Oklahoma

Gabriel A. Awejori[a], Wenming Dong[b], Christine Doughty[b], Nicolas Spycher[b], Mileva Radonjic[a*]

[a]*Hydraulic Barrier Material and Geomimicry Laboratory, School of Chemical Engineering, Oklahoma State University, 420 Engineering North, Stillwater, OK 74078, USA*

[b]*Energy Geosciences Division, Lawrence Berkeley National Laboratory, 1 Cyclotron Road, Berkeley, CA 94720, USA*

**Corresponding author: mileva.radonjic@okstate.edu*

Abstract

This study investigates geochemical rock-fluid interactions as a potential cause of rapid loss of permeability and productivity in hydraulically fractured shale reservoirs. It also interrogates the effects of these reactions in transforming depleted shale reservoirs into impermeable carbon storage units. The study employs batch reactor experiments where rock-powder samples are reacted with field fracturing fluid under reservoir temperature (95^{o}C).

Results show significant changes in mineralogy and fluid chemistry following rock-fluid reactions up to 30 days. Initial mineralogy of the rock samples includes quartz, feldspar, carbonate, pyrite, and clay minerals. Post-reaction rock mineralogy reveals the breakdown of pyrite, carbonates and feldspars, and an increase of illite content. Results from reacted fluid analyses corroborate the mineralogical changes observed after different reaction periods. Mineralogical changes in rock powders and changes in fluids chemistry at different sampling intervals (0, 7 and 30-days) reveal complex trends of dissolution and precipitation of various components. In general, the reactions proceed as follows: Dissolved oxygen and oxidants in fracturing fluids cause the breakdown and oxidation of pyrite which introduces transient and localized acidity into fluids. The transient acidity catalyzes the breakdown of feldspars and carbonates leading to the release of primarily Na, Al, Si, Fe, and inorganic C into solution. These dissolved elements subsequently react to precipitate secondary minerals which may be detrimental to reservoir permeability in the long-term. Results from experimental modelling confirmed the above-mentioned dissolution, precipitation reactions.

Findings from this research serve an essential basis to help in finetuning fracturing fluid compositions to mitigate adverse reactions that cause rapid decline in permeability and productivity in hydraulically fractured shale reservoirs. The findings also have applications in geological carbon storage in depleted shale reservoirs in context of mineralogical alterations capable of transforming these reservoirs into impermeable carbon storage units and seals.

Key Words: Shale, Carbon Storage, Hydraulic Fracturing, Geochemical Reaction, Illitization

1.0 Introduction

Exploration and development of unconventional reservoirs to meet demands for natural gas has witnessed significant growth in the last couple of decades. At the same time, the energy transition to renewable energy resources demands an urgent implementation of CO_2 storage at industrial scale. In addition, hydrogen production and storage, also require complete understanding of the subsurface geological barrier materials (Amirthan and Perera, 2023; Aslannezhad et al., 2023; Josephs et al., 2023; Olabode, 2012; Radonjic et al., 2020; Tarkowski and Uliasz-Misiak, 2022). Shale rocks are associated with a high clay content and complex microstructure, with variable pore shapes/sizes and multiscale-natural fractures, as well as compositional heterogeneity (Das et al., 2021; Guo et al., 2016; Ma et al., 2017; Xiong et al., 2022). Though the predominant minerals are quartz, clay and carbonates, other subordinate reactive minerals are present, for example pyrite, feldspars, biogenic silica, and iron oxyhydroxides. The high clay content makes shales essentially impermeable and thus difficult to produce from (Swami et al., 2012). To produce from these reservoirs, horizontal drilling and hydraulic fracturing are employed to increase fracture network and ensure sufficient permeability is generated to enhance hydrocarbon flow (Fakcharoenphol et al., 2013). Though these technologies enable production from shales, most hydrocarbons are still left unproduced due to rapid decline in permeability following hydraulic fracturing. Estimated recoveries from unconventional shale reservoirs remain low at about 10% (Mukhina et al., 2021). Due to the complex mineralogy and uniqueness of each shale reservoir, hydraulic fracturing fluids are constantly finetuned to ensure improved and sustained permeability after fracturing.

In the case of an emerging play like the Caney Shale with limited production history (Wang et al., 2021), establishing a basic knowledge of geochemical response to fracturing fluids is essential. Earlier publications on Caney and other shales report that causes of permeability loss and consequent production decline are largely attributed to geo-mechanical (Akrad et al., 2011; Crawford et al., 2018; Du, 2019; Katende et al., 2023; Lu et al., 2023) and geochemical triggers (Abbasi and Khamehchi, 2021; Awejori et al., 2024; Gundogar et al., 2021; Isah et al., 2022; Zhang et al., 2014). This study investigates potential geochemical reactions in hydraulically fractured reservoir that can cause rapid loss of permeability. This knowledge will help improve hydraulic fracturing process and ensure sustained productivity in hydraulically fractured shale reservoirs. In another context, the research provides understanding of geochemical reactions that can transform depleted shale reservoirs into carbon and hydrogen storage units as well as impermeable seals, as the two technologies are currently considered vital for effective energy transition.

2.0 Literature Review

2.1 Post-Fracturing Reactions in Shale Formations

Hydraulic fracturing involves the injection of fluids at high pressure to initiate fractures in subsurface reservoirs which will generate sufficient permeability to allow flow of hydrocarbons to the wellbore. The difference in chemistry of engineered fluids compared to formation brines and

overall formation conditions introduce chemical disequilibrium when the fracturing fluids encounter the formation. This leads to a series of chemical reactions and mineral alterations that have been observed and documented in many studies on rock-fluid geochemistry (Bratcher et al., 2021; Heidari et al., 2017; Herz-Thyhsen et al., 2019; Olabode and Radonjic, 2017; Spielman-Sun et al., 2021). Reactions can be in the form of dissolution of minerals whilst other reactions lead to precipitation of new minerals. For example, the acid fluid injected into the formation at the beginning of hydraulic fracturing leads to dissolution of minerals which in turn release high concentrations of ions into solution. As the system begins to re-equilibrate, pH changes and ionic concentration changes will then occasion the precipitation of new minerals. Some of these reactions and their ramifications are summarized in Table 1 below.

Table 1: Simplified equations of mineral dissolution due to rock-fluid reactions (Heidari et al., 2017).

Dissolution				
Minerals	**Reactants**		**Products**	**Remarks**
Pyrite	$FeS_2 + H_2O + 3.5O_2$	→	$2H^+ + 2SO_4^{2-} + Fe^{2+}$	Provide ions for precipitation of ferric oxyhydroxide and sulfate minerals
	$Fe^{2+} + 0.25O_2(aq) + H^+$	→	$Fe^{3+} + 0.5H_2O$	
	$Fe^{3+} + 3H_2O$	→	$Fe(OH)_3(s) + 3H^+$	
Calcite	$CaCO_3 + H^+$	→	$Ca^{2+} + HCO_3^-$	Dissolution of carbonates can lead to the precipitation of carbonate scales in reservoir thus reducing permeability
Dolomite	$CaMg(CO_3)_2 + 2H^+$	→	$Ca^{2+} + Mg^{2+} + 2HCO_3^-$	
Magnesite	$MgCO_3$	→	$Mg^{2+} + CO_3^{2-}$	
Siderite	$FeCO_3$	→	$Fe^{2+} + CO_3^{2-}$	
Albite	$NaAlSi_3O_8 + 8H_2O$	→	$Na^+ + Al(OH)_4^- + 3H_4SiO_4$	Dissolution of albite provides Al ions for the formation and precipitation of illite
K-feldspar	$KAlSi_3O_8 + 8H_2O$	→	$K^+ + Al(OH)_4^- + 3H_4SiO_4$	Dissolution of k-feldspar provides K and Al ions for illite formation
Geothite	$Fe(OH)_3 + 2H^+$	→	$0.25O_2(aq) + Fe^{2+} + 2.5H_2O$	These minerals mostly precipitate during and after hydraulic fracturing but can also re-dissolve and re-precipitate
Gypsum	$CaSO_4.2H_2O$	→	$Ca^{2+} + SO_4^{2-} + 2H_2O$	
Halite	$NaCl$	→	$Na^+ + Cl^-$	
Anhydrite	$CaSO_4$	→	$Ca^{2+} + SO_4^{2-}$	
Haematite	$Fe_2O_3 + 6H+$	→	$2Fe^{3+} + 3H_2O$	
Kaolinite	$Al_2Si_2O_5(OH)_4 + 6H+$	→	$2SiO_2 + 2Al^{3+} + 5H_2O$	Kaolinite can degrade to form illite
Illite	$Mg_{0.18}Fe_{0.4}K_{0.7}Al_{3.4}Si_{1.0}H_{7.94}O_{12}$	→	$0.18Mg^{2+} + 0.4Fe^{2+} + 0.7K^+ + 3.4Al^{3+} + SiO_2(aq) + 10H_2O$	Breakdown of illite provides ions which can cause precipitation of new minerals

Chlorite	$Mg_{1.04}Fe_{0.2}K_{1.28}Al_{2.24}Si_3H_{13.52}O_{18} + 10.48H^+$	→	$1.04Mg^{2+} + 0.2Fe^{2+} + 1.28K^+ + 2.24Al^{3+} + 3SiO_2(aq) + 12H_2O$	Breakdown of chlorites provides ions to form new minerals
Na-Montmorillonite	$3Na_{0.33}Al_{2.33}Si_{3.67}O_{10}(OH)_2 + 30H_2O + 6OH^-$	→	$Na^+ + 7Al(OH)_4^- + 11H_4SiO_4$	Montmorillonite can transform into illite
Ca-Montmorillonite	$Ca_{0.165}Mg_{0.33}Al_{1.67}Si_4O_{10}(OH)_2 + 6H+$	→	$0.33Mg^{2+} + 4SiO_2 + 1.67Al^{3+} + 4H_2O + 0.165Ca^{2+}$	Montmorillonite can transform into illite

2.2 Impact of Post-Fracturing Reactions on Petrophysics of Shale Reservoir

Jew et al., (2022) identified two processes of mineral precipitation which directly affects reservoir petrophysical properties and are briefly described here. These are termed based on the initiation and direction of progression of precipitation as 'matrix to fracture' and 'fracture to matrix' precipitation process. 'Matrix to fracture' type precipitation occurs due to imbibition of low ionic concentration fluids into the fracture face whilst the 'fracture to matrix' occurs due to already supersaturated fluids arriving at fracture locations.

In 'matrix to fracture' type of precipitation, high capillary pressures lead to imbibition of injected fluid into the formation matrix. The imbibed fluids, which are mostly acidic, trigger dissolution of rock minerals which eventually leads to gradual neutralization of the fluids. As the pH increases, the fluids in the matrix become supersaturated with respect to solid phase which begin to precipitate. Precipitated minerals eventually grow to occupy pores within the matrix and extend along micro and nano fractures out towards the fracture face therefore causing reduction in porosity and permeability.

'Fracture to matrix' type of precipitation is initiated when injected fluids reaching fracture face are already supersaturated. This situation results from leached ions dissolved from rock-fluid interaction when the fracturing fluid moves deeper into the formation, or when produced water is used as the base fluid for hydraulic fracturing fluids. Leaching of sulfates and other minerals from remnants of drilling fluids can also cause supersaturation of specific ions. The mineral precipitation under these conditions therefore starts from the fracture or fracture face and progressively moves through micro and nano pores into the matrix due to the extra pressure brought on by subsequent fluid injections. This leads to the blockage of micro and nano fractures linking the matrix to the main fracture.

Finally, the extent of mineral dissolution and precipitation after hydraulic fracturing is influenced by the mineralogy of the shale. For example, in carbonate-rich shales, the injected acid gets neutralized faster than siliceous-rich shales with less carbonates. In an experiment by Li et al., (2017) using the carbonate-rich Eagle Ford shale and carbonate-poor Marcellus shale, they observed that precipitated Fe(III) oxides and sulfates were more widespread in the Eagle Ford compared to the Marcellus. They opined that the high carbonate content of Eagle Ford shale

neutralized the acid spearhead thus promoting the oxidation of Fe(II) and S released during the breakdown of pyrite. The presence of specific minerals in shales can therefore determine the trajectory of geochemical reactions after hydraulic fracturing.

3.0 Materials and Methodology

This work is undertaken using Caney Shale drilled from wells in Southern Oklahoma as shown on the geological map (Fig. 1) below:

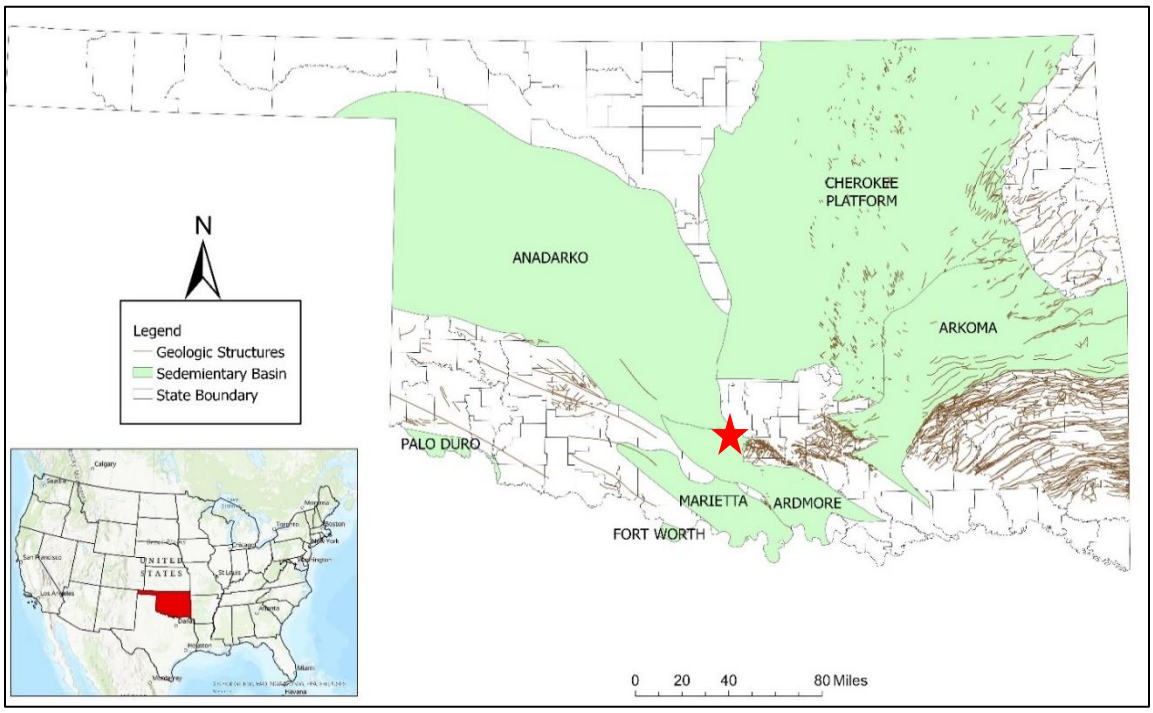

Fig. 1: Geological map of Oklahoma, showing sedimentary basins, geological structures, and location of wells (Red Star) drilled in the Caney Shale from which cores and cuttings were retrieved for this study.

3.1 Materials

Rock samples used for this study are selected at designated depths from recovered cored-rock and rock-cuttings of the Caney Shale of Southern Oklahoma. These rocks are from two different wells, one drilled vertically through designated zones of Caney Shale (Paronish et al., 2021) and the other drilled horizontally within the same part of formation where cored-rock samples are taken. Samples are labeled as Well 1 (W1) and Well 2 (W2). Well 1 refers to the vertical well that crosscuts the target zone of the formation whilst Well 2 refers to the horizontal well and runs approximately 8000ft within the target reservoir zone of the Caney Shale (Fig. 2). W1 samples are cored-rocks as shown in Fig. 3, whilst samples from W2 are rock-cuttings. All samples are taken from the same target reservoir zone within the Caney Shale. The main core where W1 samples are sampled grades from light grey (carbonate-rich) to dark grey (clay-rich) in color with depositional layering clearly visible. On several positions of the core, joints composed of mainly calcite are observed. Though W2 samples are initially mixed with drilling mud and formation

fluids, when cleaned, these samples showed similar colors as W1. The reservoir characteristics of the Caney Shale are described in detail by Andrews, (2007).

Fluids employed in this study are fracturing fluids collected from the field and deionized (DI) water as control. Table 2 shows initial fluid samples composition used in the experiment. Fluids used in these experiments are not acidized and their initial pH is circum-neutral.

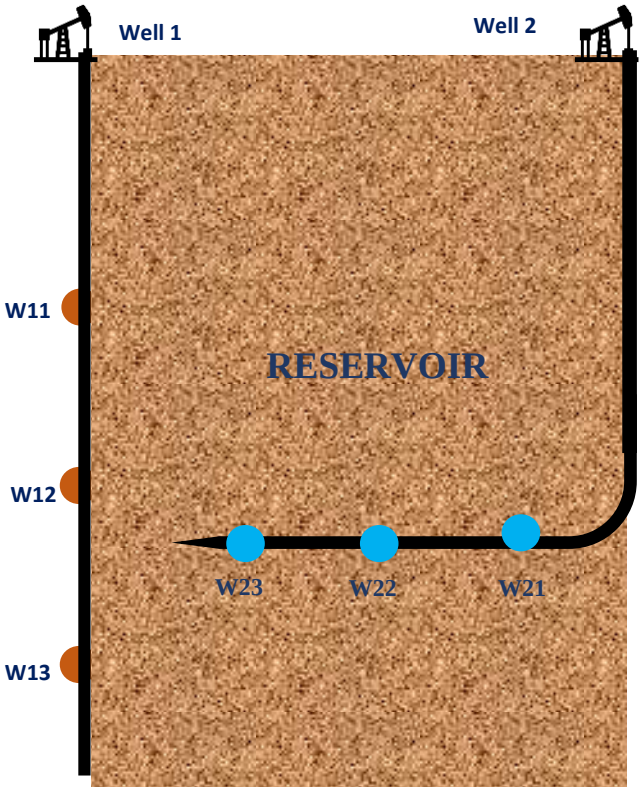

Fig. 2: Schematic showing the sampling locations in W1 (vertical well) and W2 (horizontal well).

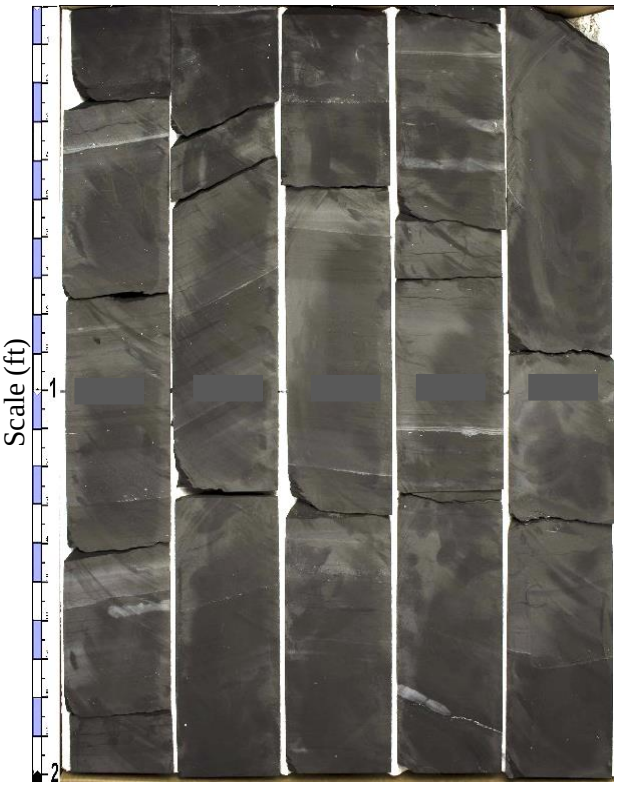

Fig. 3: Cored rock from well drilled through Caney Shale on display.

Table 2: Initial chemical composition of fluids used in experiments.

	Fluid Compositions
Case 1	Fracturing Fluid, pH ~7 (Composed of following in mass percent: 76.4% of water, 22.5% of proppant, 0.46% of Etching agent, 0.08% of friction reducer, 0.21% of gelling agent, 0.2% and 0.13% of H_2S scavenger)
Case 2	DI water, pH ~7, supplied by CEAT OSU.

3.2 Sample Preparation for X-ray Diffraction (XRD)

Given that the samples are obtained in different forms, sample preparation is conducted to get samples in powdered state for experiments. The procedure applied to prepare cored-rock is significantly different from rock-cuttings. Cored-rock is recovered from well as 4-inches diameter cylindrical core. Samples are taken at selected depths as 1inch x 2inch core plugs from the original

4-inch core using core plugging mill that employed liquid nitrogen and bit coolant. The core plugs drilled out of the target depths are then crushed into smaller chippings with a hammer before they are ground to powder using a Spex Ball Mill. On the other hand, rock cuttings from selected depths are collected in sampling buckets from the field. At the point of recovery, these samples are mixed with mud and produced fluids and therefore need cleaning. To clean the samples, small quantities (quarter of a liter by volume) of the chippings mixed with crude and mud, are sampled into 2-liter beakers. Diesel is added to the cuttings swirled at high speed for 15 minutes before it is decanted. This process is repeated until the cuttings are clean of the crude and mud. Once the cuttings are sufficiently cleaned, they are washed with acetone by the same process as done for the diesel and left to dry for three days. Finally, the cleaned rock cuttings are selected by hand-picking them out from debris still left after the cleaning processes. These cuttings are ground to powder using a Spex Ball Mill. Final preparation of both sets of samples is achieved by micronizing with a McCrone Micronizer to reduce the particle size to particles passing 34-mesh size (100µm).

3.3 Experiment

Experiments for this study are batch reactor experiments, designed to replicate subsurface conditions that drive chemical reactions between formation fluids, formation rocks and injected hydraulic fracturing fluids. In this regard, temperature, time, and surface area are regulated to mimic subsurface conditions. However, the amount of oxygenation of fluids is difficult to control. Temperature of oven where experiment is being undertaken is set at 95^{o}C and monitored throughout the period; The time for experiments are 7-days and 30-days after which samples are prepared for post-experiment analyses; Comminution of samples to particle sizes passing 34-mesh size helps to control sample size; Exposure of fluids to the atmosphere cause oxygenation but the extent of this could not be quantified. The effect of pressure on reactivity is not considered in this study.

Pyrex media storage bottles having a volume of 250mL with tight seals and capable of withstanding dry temperatures up to 180^{o}C (356^{o}F) are used in the experiments. The bottles are placed in a heat-resistant container and put in the oven for the duration of the experiments. The oven temperature is checked daily to ensure no fluctuations occurred without detection.

Rock (shale) samples are comminuted to increase the surface area reacting with the fracturing fluids. The initial fracturing fluid to rock ratio in this experiment is 150mL of fracturing fluid to 1g of powdered rock. Fluids are separated from rock powders and filtered with a 0.22µm filter into plastic bottles for further analysis during each sampling period. The sampling process lasts about three (3) minutes. The rock powders are dried and stored in glass vials waiting XRD analyses whilst fluid samples are stored in a refrigerator pending ICPMS analyses. The schematic on Fig. 4 summarizes the general workflow of the experiments, data acquisition and data analyses and interpretation whilst Table 3 shows rock-fluid samples mix list.

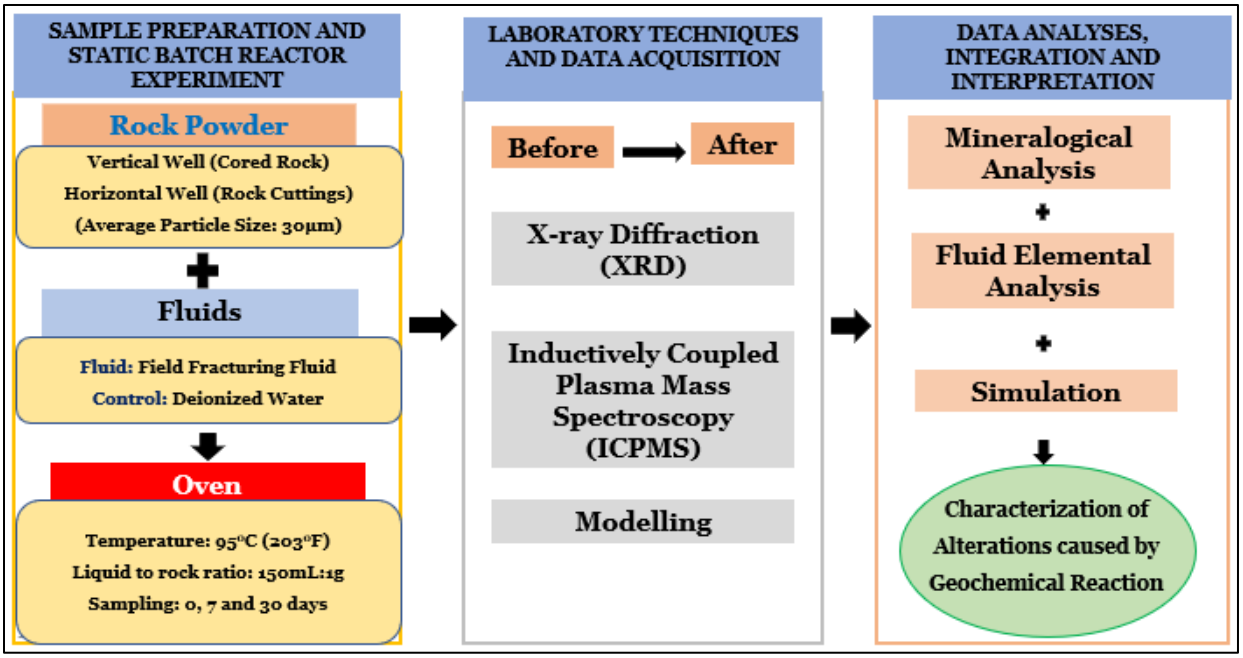

Fig. 4: Schematic showing the experimental design and analytical methods employed in the study.

Table 3: Samples and Reaction Program used for Experiment.

Sample	Type	7-days		30-days	
		Fracturing Fluid	Deionized Water	Fracturing Fluid	Deionized Water
W11	Cored Rock		×	×	
W12	Core Rock	×		×	×
W13	Core Rock	×		×	×
W21	Rock Cuttings	×		×	
W22	Rock Cuttings	×	×	×	
W23	Rock Cuttings	×		×	

3.4 Analytical Methods

X-ray Diffraction (XRD) is employed in the analysis of the mineralogical compositions and weight percentages of minerals in the rock powder samples whilst Inductively Coupled Plasma Mass Spectroscopy (ICP-MS) is used to measure the elemental concentrations in fluids. The XRD analysis is conducted with the Bruker D8 advanced X-ray Diffractometer with a Lynxeye detector. Scanning is run for 2-theta angle of 5 to 80 degrees using a step-size of 0.01-degree and a dwell time of 0.5 seconds. The semi-quantification of mineralogical contents is undertaken with BRUKER's Diffrac.suite eva software. To measure elemental concentrations in fluids, an Advanced Agilent 8900 triple Quadrupole Inductively Coupled Plasma Mass Spectrometry system (Agilent 8900 QQQ ICP-MS, Agilent Technologies) is used. Analytical methods and instrument settings used in this work are comparable to those reported in Belkouteb et al., 2023 and Agilent

application notes (Agilent, 4th Edition). pH measurements are conducted with an Oakton pH 150 meter where each fluid pH was calculated as the average of three measurements.

3.5 Modelling

The modelling of experiments is undertaken with three essential components including the TOUGHREACT v4.13 simulator (Sonnenthal et al., 2021; Xu et al., 2011), the thermodynamic database, Thermoddem (Blanc et al., 2012) and EOS3, an equation of state module (Pruess et al., 1999). Two major sets of simulations are run, including Caney Shale with fracturing fluids (FF) and then Caney Shale with deionized water (DI). The simulation took cognizance of the headspace in the reaction bottle and the potential of oxygen being drawn into this space as well as the interference of oxygen during sampling. In this regard, several simulations are run to evaluate different oxidizing conditions. This is mainly achieved by varying the concentration of atmospheric oxygen drawn into the reaction bottle during sampling until the best match with the experimental data is achieved.

The content of the three common carbonate minerals identified in the Caney shale, namely calcite, dolomite and ankerite, are also adjusted to enable the model to best match the experimental data. These adjustments are done in such a way that the total carbonate content identified in XRD analysis remains unchanged. Another key parameter that is adjusted for the various simulations is the reactive surface areas of the minerals. All these are (loosely) calibrated to get the best fit with experimental data where deionized water is used as reaction fluid. These calibrated values are subsequently used to model experiments with fracturing fluid. The simulation incorporated the effects of cation exchange applying data from Appelo and Postma (2005) in addition to the mineral dissolution and precipitation dynamics.

In characterizing the mineralogy of the Caney shale used in simulation, the results from XRD analysis of the samples are used. These results are augmented by geochemical modelling to assign specific clay minerals from the thermodynamic database to the unspecific ‘illite/smectite’ amounts evaluated from the XRD analysis. Albite content determined from XRD analysis is modelled as a low-Ca (An10) plagioclase utilizing data from Arnorsson and Stefansson (1999) adjusted for consistency with the Thermoddem database. Additionally, trace amounts (~0.5%) of alkali-feldspar, chlorite, and organic carbon (modelled as elemental C), which is below the detection limit of the XRD technique are assumed to be present in the Caney shale for the purpose of simulation. This assumption is premised on the fact that these minerals have generally been reported in the Caney shale (e.g. Grieser et al., 2007). It is worth stating here that thermodynamic data for ankerite in the simulation are taken from Holland and Powell, (1998) since these are unavailable in the Thermoddem database. Table 4 shows the specific phases of the minerals used in the modelling.

The elemental concentrations of the fracturing fluid from ICPMS analysis, industry data (FracFocus) and other assumptions served as the bases for estimation of simulated fluid composition shown on Table 5.

Table 4: Solid phases used in geochemical modelling.

Shale Minerals	
K-feldspar (Microcline)	Illite(Mg)
Albite (Ab90An10-low)	Calcite
Montmorillonite (MgMg)	Dolomite
Ankerite	Pyrite
Chlorite (Cca-2)	C(element)
Potential Secondary Minerals	
Gibbsite Boehmite Ferrihydrite(2L) Chalcedony	
Siderite	
Kaolinite	

Table 5: Composition of fracturing fluid used in modelling the experiments.

Component	**Value**	**Source/Assumption**
pH	7.05	Measured
	(ppm)	
Cl-	146	From charge balance
SO4--	34.0	Obtained from FracFocus ammonium persulfate 156 ppm, which was lowered to yield barite equilibrium
HCO3-	5.21	Constrained by log(*f*CO2)=-3.4 (atmospheric)
Si	6.01	Obtained from ICP-MS analysis
Al+++	9.07E-05	Obtained from ICP-MS analysis at 0.273 ppm, and was then constrained by kaolinite equilibrium
Ca++	64.6	Obtained from ICP-MS analysis
Mg++	22.8	Obtained from ICP-MS analysis
Fe++	0.0359	Obtained from ICP-MS analysis
K+	3.61	Obtained from ICP-MS analysis
Na+	66.6	Obtained from ICP-MS analysis
B	0.391	Obtained from ICP-MS analysis
Sr++	0.883	Obtained from ICP-MS analysis
Ba++	0.103	Obtained from ICP-MS analysis
HPO4--	13.1	Obtained from ICP-MS analysis of P
O2(aq)	129	Constrained by log(*f*O2) = -0.7 (atmospheric)
Acetate-	65.6	Obtained from FracFocus acetic acid

4.0 Results

In this section, mineralogy of the samples before and after reacting with fluids for both sampling periods are compared to identify mineralogical changes that occurred due to reactions. Results from pH measurements and reacted fluid analyses are then presented, while the last part of this section summarizes modelling results.

4.1 Mineralogy of Initial versus Reacted Samples

Initial mineralogy of all the samples from the two wells are similar, consisting of quartz, illite, albite, dolomite, calcite, and accessory minerals in various percentages. Reaction with fracturing fluids caused changes to the mineralogy of the rocks. These changes follow comparable trends with slight variations that occur as a result of the differences in initial mineralogy of samples. The fracturing fluid used in this study has circum-neutral pH, therefore carbonate dissolution is slower compared to earlier experiments reported in Awejori et al., (2022) where fluids are acidized to initial pH of 4. These experiments are designed to represent later stage reactions in the deep fracture system of the reservoir where the effect of initial acid spear is minimal.

In general, pyrite and dolomite dissolution occur in rock samples during rock-fluid interaction. Based on trends observed from bar graphs in Fig. 5 and Fig 6 respectively, it is hypothesized that pyrite dissolution occurs first due to contact with oxidized fluids. The dissolution of pyrite generates transient acidity (due to the generation of sulfuric acid) in the fluid and triggers the localized dissolution of dolomites (carbonates).

The general trend of albite shows a gradual dissolution of albite in most but not all samples, possibly to form illite. The amount of quartz, which is least reactive, would be expected to remain essentially constant over the reaction period. However, the decline in quartz percent weight in some samples after 7-days may be due to dissolution of microcrystalline quartz which has a biogenic origin and is less stable. Increases in quartz percent weight in some samples after 30-days are the effects of renormalization of the percent weights following dissolution of other minerals. Though one would expect the illite content to decrease due to breakdown, in most of the experiments, the illite content increases within the first 7-days and reduces or remains constant between 7-days to 30-days. The increased illite content is likely the result of albite (plagioclase) alteration, although one cannot rule out sample heterogeneity masking the effects of rock-fluid interactions or the renormalization of mineral weight percent following dissolution of pyrite, dolomite, and feldspar. Another key observation from XRD measurements is the increased amorphous content after reaction as shown in Fig. 7. These increases are particularly prominent within lower 2-theta angles related to clay minerals which gives an indication that these entities originate from the clay minerals.

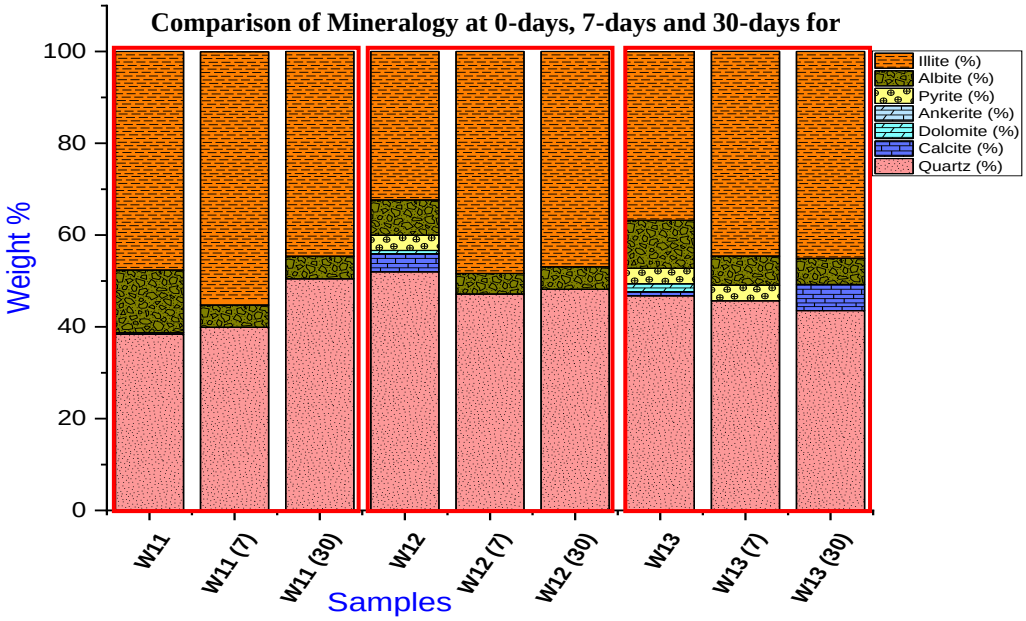

Fig. 5: Bar chart comparing mineralogical compositional evolution of vertical well samples. Samples with extension (7) represent samples after 7-days reaction and those with (30) represent 30-days reaction.

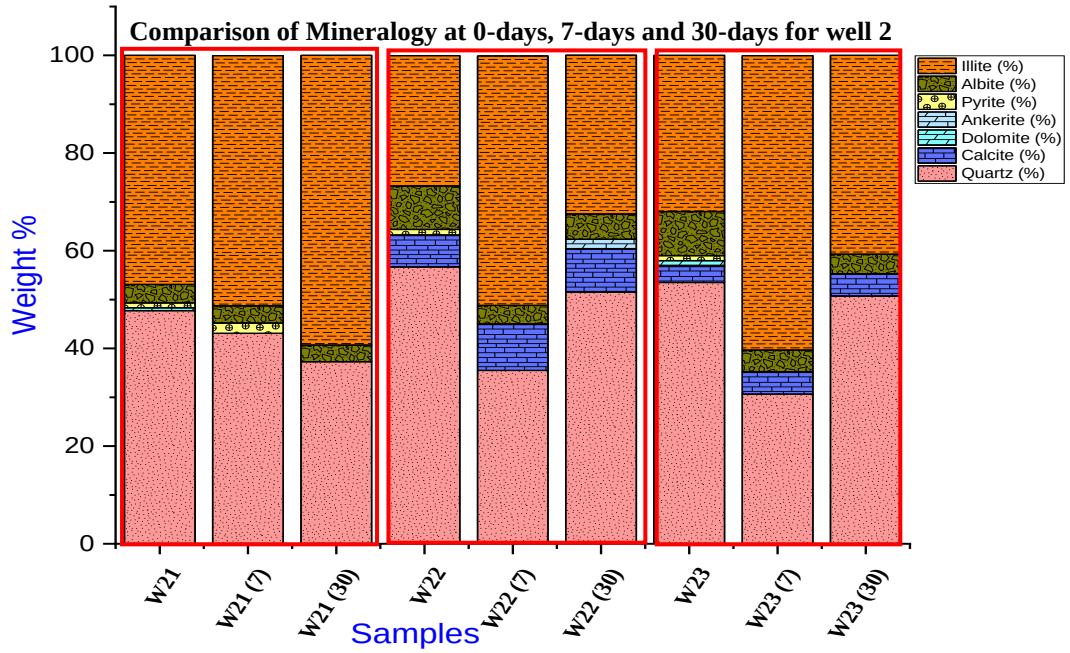

Fig. 6: Bar chart comparing mineralogical compositional evolution of horizontal well samples. Samples with extension (7) represent samples after 7-days reaction and those with (30) represent 30-days reaction.

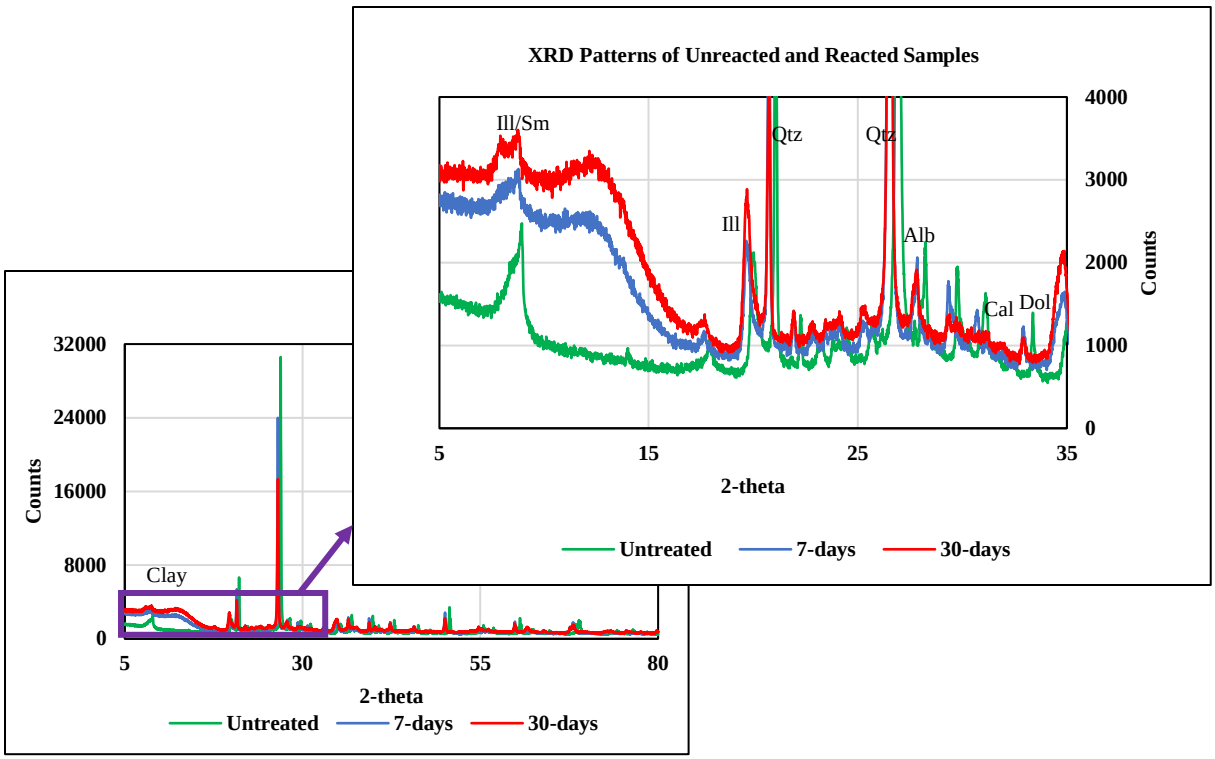

Fig. 7: XRD diffractogram showing increased amorphous content after reaction of rock-powders with field-fracturing fluid. The increased amorphous content is indicated by the bulging at the base and reduction in sharpness of peaks (Alb – Albite, Cal – Calcite, Dol – Dolomite, Ill - Illite, Sm – Smectite, Qtz – Quartz)

4.2 Reacted fluid Analyses

4.2.1 pH Evolution

In this experiment, the initial pH for fracturing fluid is circumneutral, thus reactions are not expected to proceed as observed in experiments where the initial pH of fluid is lowered by addition of acids (Edgin et al., 2021; Harrison et al., 2017; Marcon et al., 2017). The fluid is not acidized because this study is designed to monitor the reaction of fluids in the subsurface after acid has been exhausted. The pH of samples shows marginal increases over the reaction period though the trend shows a drop between 7-days to 30-days. The pH of reacted fluids is generally less than 8, though sample W22 after 7-days reaction is an outlier (as shown in Table 6).

Table 6: pH of initial fracturing fluid compared to pH of reacted fluids at 7-days and 30-days.

pH Evolution of samples			
Sample	**Initial**	**7-days**	**30-days**
W12	7.05	7.73	7.53
W13	7.05	7.90	7.75
W21	7.05	7.71	7.53
W22	7.05	8.86	7.71
W23	7.05	7.32	7.72

4.2.2 Si Concentration

Silicon (Si) concentration in reacted fluid is expected from the dissolution of quartz and amorphous silica polymorphs, plagioclase dissolution, and desorption/ion exchange from clay minerals. The stability of quartz and the initial circumneutral pH of fluid used for the experiments portends minimal breakdown of quartz. Therefore, the concentration of Si in reacted fluids would be expected to be low. However, the observed concentrations of Si (Fig. 8) are significantly above the quartz solubility. The dissolution of feldspar and exchange at clay sites therefore account for major part of the Si in reacted fluid. A more significant component of the Si in solution may be contributed from the dissolution of undetected biogenic silica and microcrystalline quartz which typically form in the shallow ocean depositional environment of the Caney Shale (Fritz et al., 2012).

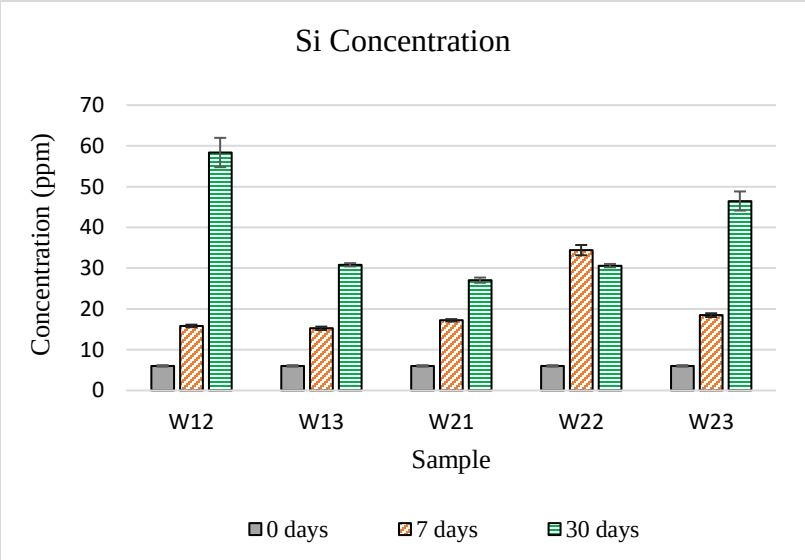

Fig. 8: Trends of Si concentration in fluid over reaction period. The trajectory shows increased Si concentration in effluent over time, due to breakdown of feldspar, microcrystalline quartz, clay minerals, and biogenic silica all of which contain Si.

4.2.3 K Concentration

The potassium (K) concentration increases in the reacted fluids (Fig. 9) is mainly from the feldspar dissolution and from ion exchange in clays. The breakdown of potassium feldspar and clay minerals during reaction releases potassium into solution. These K ions are subsequently absorbed into clay interlayers to stabilize them. Stabilization of clay interlayers by K ions can significantly minimize further ion exchange thus the marginal changes in K concentrations for most samples after 7-days and up to 30-days. Illite, the predominant clay mineral in the rock formation is mostly stabilized by absorbing K cations into its interlayer. The size of the K cations keeps them fixed in the clay interlayer thus stabilizing the clay and preventing further ion exchange. Marginal differences in K concentration between various samples are likely related to mineralogical heterogeneity between samples.

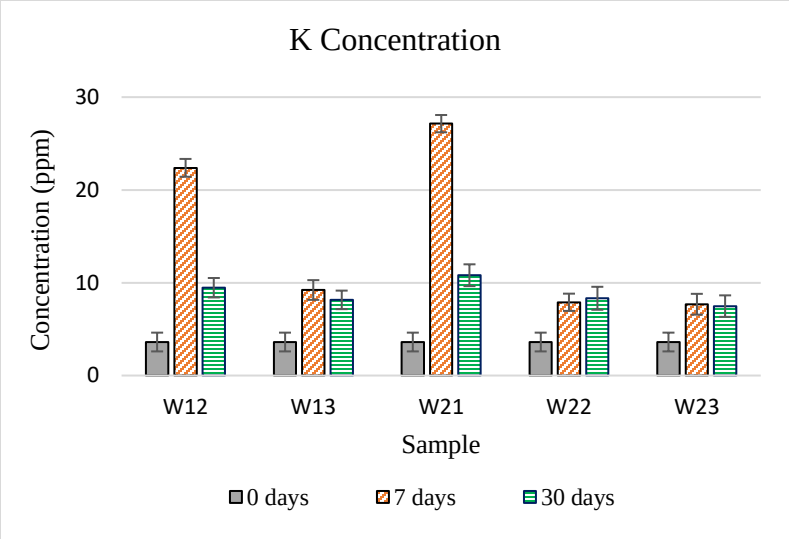

Fig. 9: Trends of K concentration in fluid over reaction period. The initial spike of K in fluid for some samples at 7-days is due to dissolution of feldspars and high desorption from clay surfaces. K is subsequently absorbed into clay interlayer to stabilize clays.

4.2.4 Ca Concentration

The calcium (Ca) concentration in reacted fluids is relatively stable throughout the experiments. There are, however, marginal increases in Ca concentrations in all the reacted samples, though this increase is delayed for some of the samples as observed in Fig. 10. The small changes in Ca concentrations may be due to the near neutral pH of the fracturing fluid used for experiments which induces minimal carbonate dissolution. However, the oxidative dissolution of pyrite could cause a transient acidity in the reacted fluid, leading to more dissolution of carbonates and the observed small increases in Ca concentrations. Adsorption and desorption of Ca at clay exchange sites may also be responsible for the small fluctuations in Ca concentration in reacted fluid.

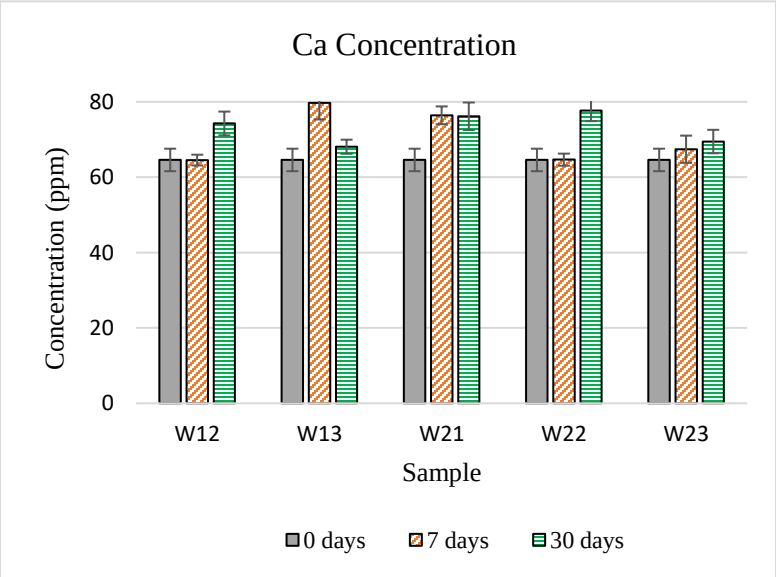

Fig. 10: Trends of Ca concentration in fluid over the reaction period. The increase in Ca concentration is mainly due to dissolution of carbonates which is slow because of the circumneutral state of initial fluid.

4.2.5 Na Concentration

For both W1 and W2 samples, the sodium (Na) concentration in reacted fluids increased after the first 7-days. Though concentrations increased marginally in W1 between 7-days to 30-days, W2 samples maintained similar concentrations or witnessed a slight drop as observed in Fig. 11.

Increases in Na concentrations are likely from the dissolution of albite/plagioclase feldspar whilst cation exchange and desorption from clay sites may also contribute to these concentrations. Cation exchange initiates immediately following mixing of rock powders and fluids and is presumably the highest contributor to sodium in solution within the first days (day 0 – day 7). Dissolution of albite also contributes to Na concentration though this process will tend to be slower than cation exchange in clays. The marginal drop in Na concentration after 30-days in some samples may be due to re-adsorption of free sodium on clay surface or formation of Na minerals. However, this will need to be further investigated for experimental confirmation, applying surface chemistry analysis such as XPS (x-ray photoelectron spectroscopy).

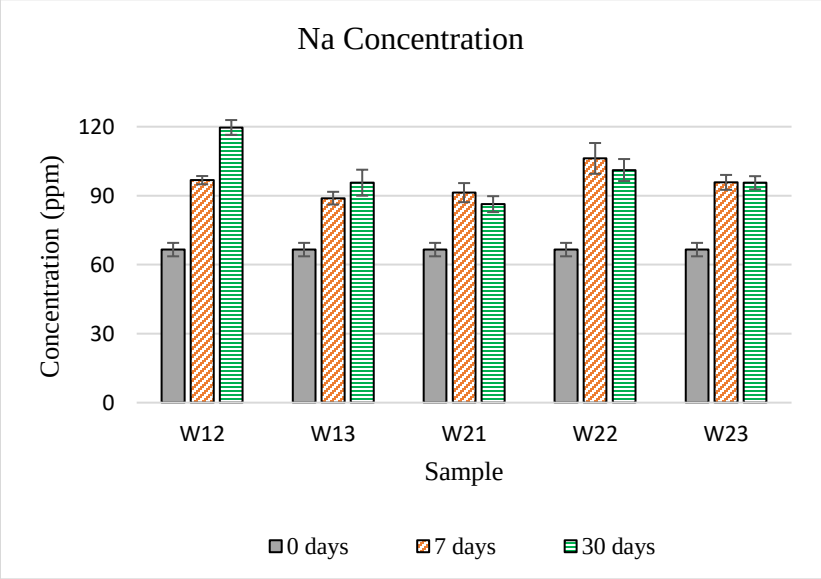

Fig. 11: Trends of Na concentration in fluid over reaction period. Increase of concentration over time is due to mineral dissolution and exchange at clay sites. The marginal drops are due to re-adsorption to clay minerals.

4.2.6 Mg Concentration

Magnesium (Mg) concentration trends shown in Fig. 12, during rock-fluid reactions are mainly attributed to the dissolution of dolomite and cation exchange in clays. Mg ions exchange is mostly absorbed and adsorbed by clays rather than being released in solution. From the graph, it is observed that Mg concentrations showcase a generally decreasing trend. The decrease in concentration can also be due to precipitation of secondary Mg-bearing minerals, although these

might be present in low amounts as XRD analysis did not provide such supporting results. This would need to be further investigated in future experiments, such as flowthrough rock core, where tools such as Electron microprobe analyzer can be deployed to detect low elemental concentrations in rock formations (in ppm).

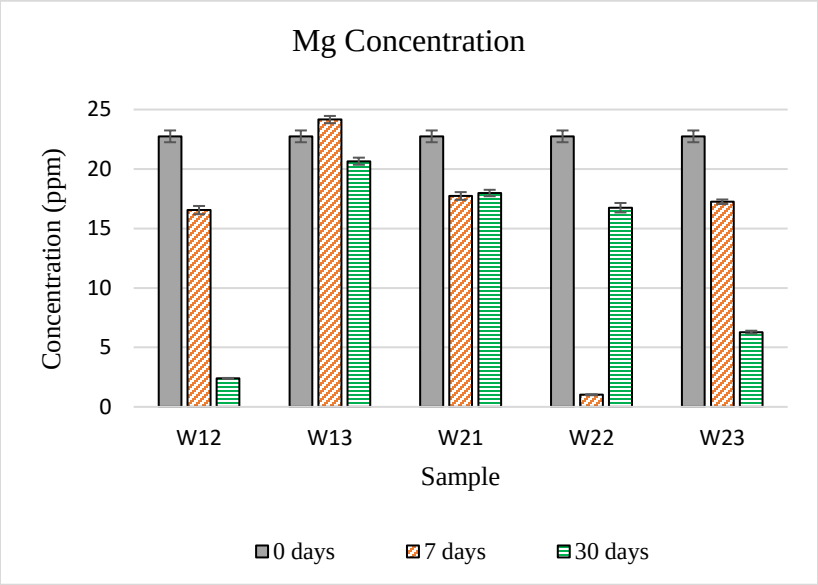

Fig. 12: Trends of Mg concentration in fluid over reaction period. The general drop in Mg after reaction is due to precipitation of Mg bearing minerals but in low amounts, thus undetectable by XRD.

4.2.7 Al Concentration

Aluminum (Al) in reacted fluid is mainly from the dissolution of feldspars and release of Al due to exchange in clay sites. The formation of clays and precipitation of Al-based minerals are responsible for decreasing trends of Al in reacted fluids shown in Fig. 13. Trends in Al concentration show marginal increase in Al concentration in some samples after 7-days which subsequently drops to pre-reaction concentrations in fluid. The increase of Al occurs when rate of feldspar breakdown and release from clay sites is higher than precipitation of Al-based minerals. Al ions however can also exchange for Si ions in clay sites, thus absorption by clays.

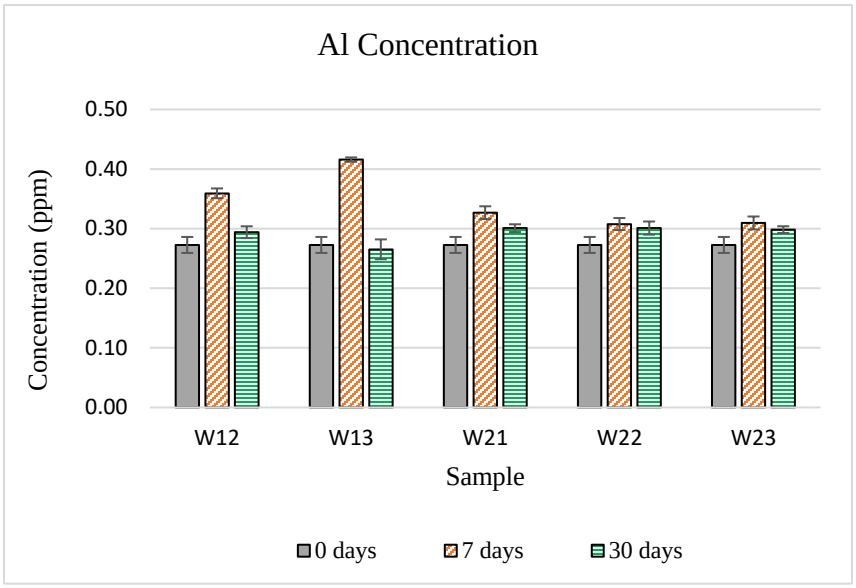

Fig. 13: Trends of Al concentration in fluid over reaction period. The initial increase in Al is mainly due to Feldspar dissolution whilst precipitation of Al-bearing minerals like illite (clay) is responsible for the decline in the latter times.

4.2.8 Fe Concentration

Iron (Fe) in reacted fluid is mainly from the dissolution of pyrite and Fe-bearing carbonate minerals, and possibly also release from clay exchange sites. Dissolution of pyrite in the presence of oxidized fluids is, however, expected to be an important contributor of Fe in solution, at least initially. From the trends observed in Fig. 14, Fe concentration in reacted fluid for all samples increases in the first 7-days of reaction and then drops going to 30-days. The initial increase after 7-days is mainly due to breakdown of pyrite while the decrease afterwards is from precipitation of Fe-based minerals, mostly ferric-hydroxides which are generally detrimental to formation permeability.

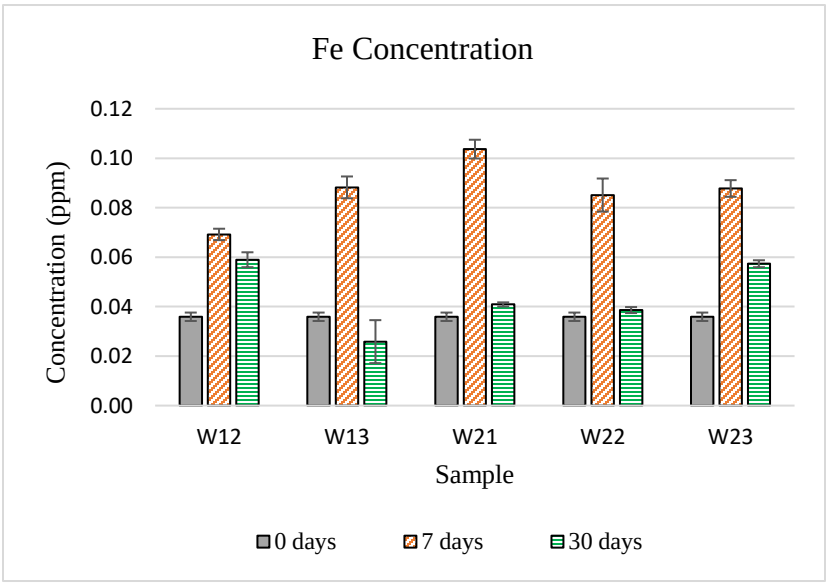

Fig. 14: Trends of Fe concentration in fluid over reaction period. Initial spike in Fe concentration is due to breakdown of Fe-bearing minerals which are subsequently taken up during precipitation of Fe minerals like Fe (III) oxides.

4.2.9 Sr Concentration

Strontium (Sr) is typically associated with carbonate minerals and adsorbed to clay surfaces; thus, it enters solution as a result of dissolution and cation exchange at clay sites. Sr in solution subsequently reacts with sulfate to form Celestine ($SrSO_4$) which serves to occlude flow pathways in formation (Jew et al., 2020). Elemental analyses of reacted fluid in Fig. 15 show marginal increases in Sr concentration for 7-days of reaction and a decrease for some samples after 30-days. The release of Sr from clay sites is responsible for the increase and the subsequent precipitation of $SrSO_4$ leads to reduction in Sr concentration in reacted fluids. Samples with increasing concentration of Sr may be due to delayed release of Sr into solution or unavailability of sulfate for precipitation.

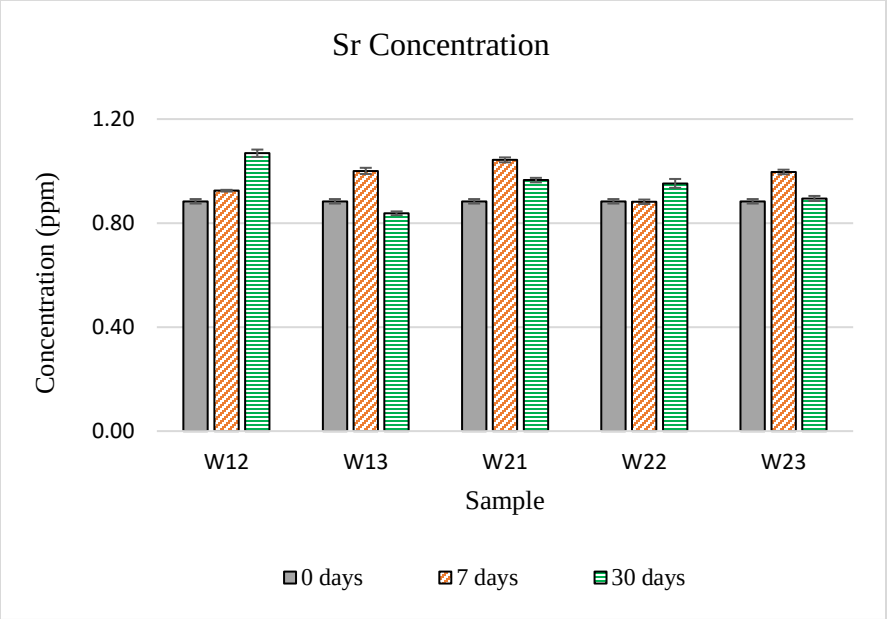

Fig. 15: Trends of Sr concentration in fluid over reaction period. Release of Sr adsorbed to clay causes increased concentration in fluid but precipitation of celestite and strontianite causes marginal drop in concentrations.

4.2.10 Ba Concentration

Barium (Ba) is usually adsorbed to clay surfaces and released into solution due to exchange of cations at clay sites (Renock et al., 2016). Ba in solution subsequently reacts with sulfate to form barite which is deleterious to formation petrophysical properties (Osselin et al., 2019). Trends of Ba concentrations in reacted fluids (Fig. 16) could be explained by release of barium from clay sites during initial reaction and subsequent adsorption of Ba in clays formed or precipitation of barite.

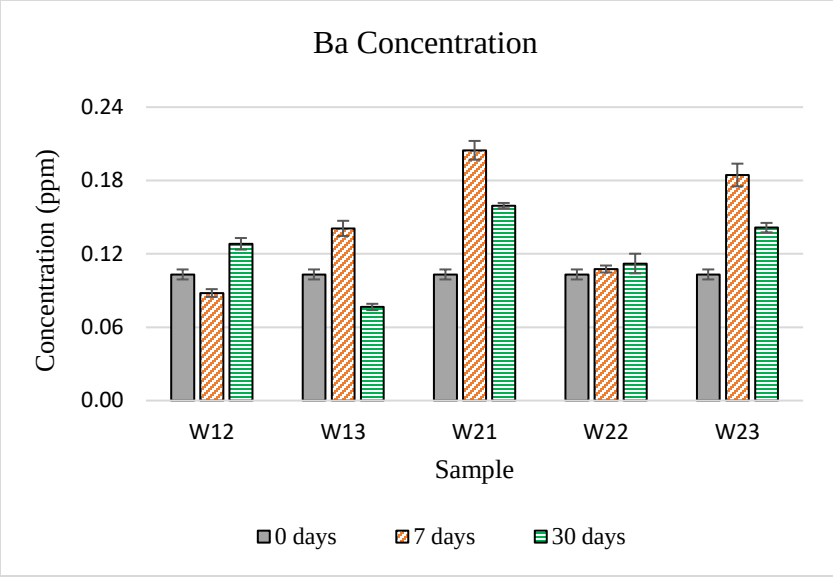

Fig. 16: Trends of Ba concentration in fluid over reaction period. Increased concentrations after 7-days indicate periods of desorption of Ba from clay sites whilst later stage reduction may be caused by precipitation of barite.

4.3 Simulation Results

The results obtained from the geochemical model of the experiment generally agree with data obtained from experiments (Fig. 17). The trends observed in modelling of fracturing fluid are similar to that observed with deionized water. It is however worth stating that several assumptions were made in the model concerning the constraining of initial rock and fluid properties. These include the determination of fracturing fluid composition and elemental concentrations, redox conditions of the fracturing fluids, composition and amounts of trace minerals in shales, reactive surface areas of minerals (these are calibrated based on the experiments with DI water) and the input thermodynamic data.

The modelling showed increased Ca concentration in fluid to emanate from calcite dissolution. The dissolution of calcite is initiated due to pH decrease which is driven by the oxidation of pyrite (and to a lesser extent carbon). Based on the model, the oxidation of pyrite and dissolution of ankerite are the main contributors to Fe concentrations in fluids. Fe is however consumed in the precipitation of ferrihydrite and to a minor degree chlorite. Mg concentration in fluids which is mainly from the breakdown of dolomite and exchange from clay sites follow similar trends as Fe and is consumed in the precipitation of secondary minerals, mostly chlorite. Minor precipitation of illite, montmorillonite, and kaolinite occurs only with shales of high (>10%) plagioclase content, accompanied with gibbsite.

When the plagioclase content of shale in the model is low, illite breakdown occurs even at high rates of K-feldspar dissolution. Though the model shows that Na and K in the fluid are from the dissolution of plagioclase and k-feldspar respectively it is unable to reproduce the trends of K concentration observed in the experimental data unless the dissolution rate of K-feldspar is

increased by four orders of magnitude above known rates of K-feldspar dissolution. The inability of model to reproduce the trends of K yield into solution could still be attributed to the underestimation of K release from ion exchange or overestimation of the stability of K-feldspar, or combination of both processes in the model. These are, however, unlikely.

The oxidative dissolution of pyrite and ankerite followed by precipitation of ferrihydrite in the model is consistent with results from experiment which shows an initial increase in dissolve Fe concentration in fluid with subsequent decline of the Fe in the fluid. The reprecipitation of dissolved Al to Al-hydroxide (which is modeled as gibbsite) in the model, makes the Al concentrations in the fluids generally underpredicted. These trends of Al concentrations in the model are therefore explained by two possibilities. The first is that gibbsite precipitation occurs at extremely high rates and the second is that the secondary phase precipitated is not gibbsite.

It is worth noting that modeled trends of pH, Fe, Ca, and Mg are sensitive to the degree of oxidation considered in the simulation as well as the proportions of various carbonate minerals considered in the simulation.

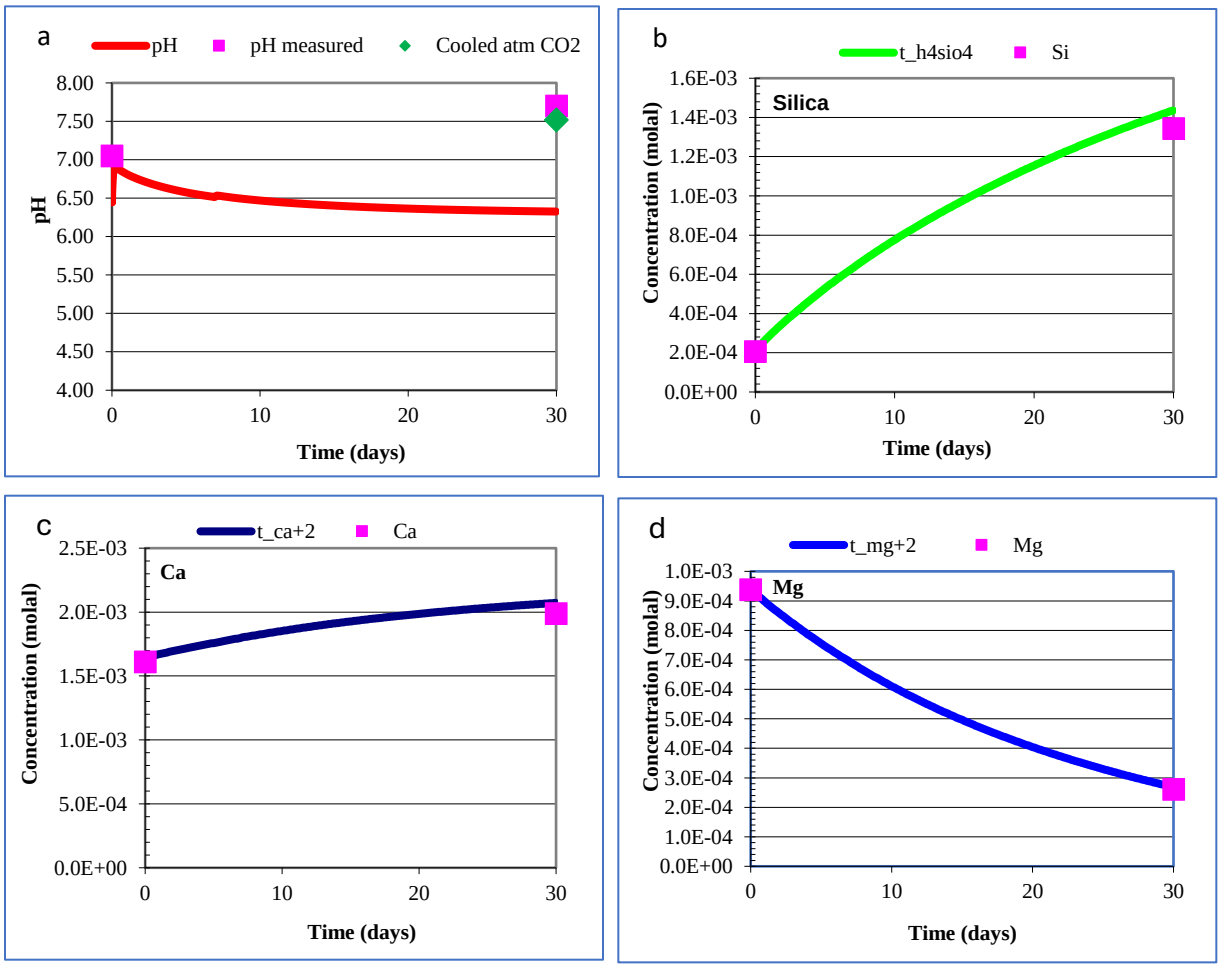

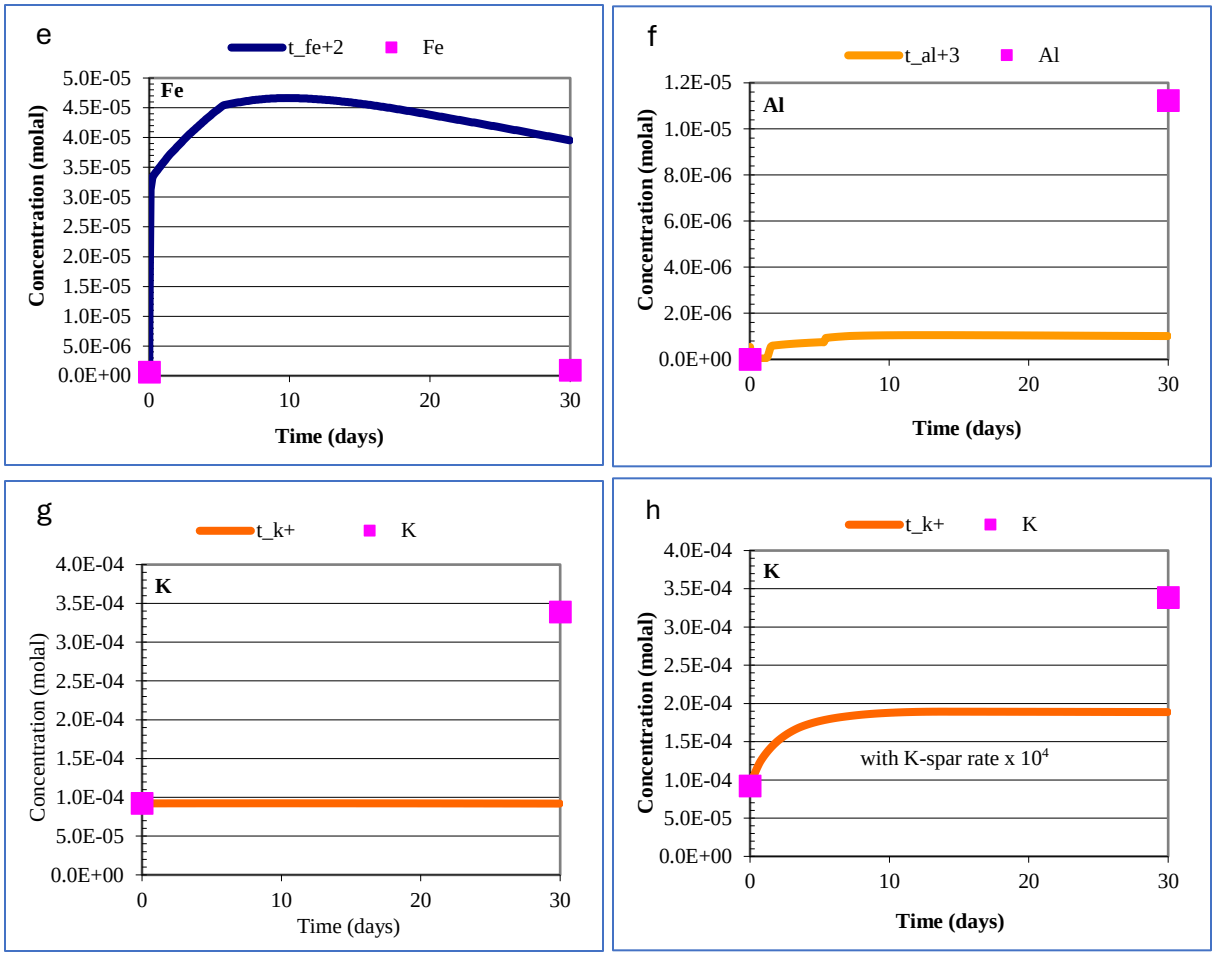

Fig. 17: Comparison of fluid compositions and concentrations obtained from modelling (lines) and measured from experiment (squares) (Sample W11). The final modelled pH (at 95°C) is numerically cooled to 25°C (diamond symbols) for comparison with the measurements.

5.0 Discussion

In this section, the results observed above are discussed in context of existing studies and potential reactions based on trends in mineralogical changes and elemental concentrations in reacted fluid.

5.1 Illitization

Illitization refers to the formation of illite and is a crucial process that occurs during diagenesis of rock formations. This phenomenon witnessed substantial attention from researchers because of its impact on hydrocarbon generation and migration and reservoir petrophysics (Berger et al., 1997; Lázaro, 2007; Ohazuruike and Lee, 2023). In recent times, illitization has been reported to play a significant role in post-fracturing rock-fluid interactions (Credoz et al., 2011). The prime source of illite formation being the breakdown of feldspars and the transformation of smectite to illite.

Experimental studies that suggest illitization in post-fractured reservoir are summarized as follows. Credoz et al., (2011) reacted k-feldspar and illite/smectite mixed layer clays with 0.1 NaCl at 80°C within pH ranges of 3 to 8.5 and observed that illitization of smectite occurred. The illitization was

particularly intense within acidic pH and moderate at neutral pH. They described the illitization at the acidic pH as proton-promoted illitization whilst the illitization at neutral conditions was attributed to thermal effects. Huang et al., (1986) investigated the dynamics of illitization during rock-fluid geochemical reactions where they reacted plagioclase feldspar with minor impurities (mica) and 1M KCl at 200^{o}C and 500bar. The initial pH and fluid/rock ratios were varied for the various experiments. They premised their investigation on findings by Güven et al., (1982) that the nucleation and growth of illite occurs under neutral conditions with high fluid/rock ratios and high Al concentrations in the fluid. In their study however, they observed that illite formation required specific order of processes though they confirmed the findings of Guven et al., (1982) that the formation of illite is favored by high Al concentrations at near-neutral pH conditions in 1M KCl solutions. Huang et al., (1986) revealed that to obtain thermodynamic conditions most suitable for illite formation, an initially highly acidized fluid environment is needed to yield high Al concentration in solution and then subsequent titration to obtain a high fluid/rock ratio ensures the circum-neutral conditions in reservoir environment necessary for illite formation. These processes and kinetics in formation of illite are identified to exist during hydraulic fracturing or treatment of reservoir for enhanced hydrocarbon recovery.

In the current study, illite weight percent increases in the first 7-days of reaction and reduces or remains constant in various samples between 7-days and 30-days. Though the pH of fluid is not initially within the acidic range, the breakdown of pyrite can cause localized transient acidity in the fluid which leads to dissolution of feldspar to generate enough Al in solution thus triggering illitization. The Al concentrations reduce over time and between 7-days and 30-days, there is not enough Al for illitization to continue, therefore the stable or reduced compositions of illite in samples between 7-days and 30-days.

5.2 Mineral Precipitation and Scale Formation

5.2.1 Iron Oxidation and Precipitation

Iron oxidation is one of the most common reactions during hydraulic fracturing (Harrison et al., 2017). During breakdown of pyrite, iron is released as Fe(II) and subsequently oxidized to Fe(III). In addition, Fe(II) can also be released from sites in clay minerals, Fe in carbonates (e.g. siderite, ankerite) or from organic matter which are oxidized by available oxygen from fracturing fluids. At low pH, iron has less of a tendency to oxidize than at high pH. This led to an initial conclusion that oxidation of iron at low pH conditions is negligible. However, research has shown that there is significant iron oxidation even under acidic conditions below pH of 2 (Awejori et al., 2022; Alalli et al., 2018; Gundogar et al., 2021; Harrison et al., 2017). Presence of organic phases have also been identified to accelerate the oxidation of Fe(II) to Fe(III), especially under acidic conditions (Jew et al., 2017). This has implications on fracturing of shale reservoirs as the presence of hydrocarbons essentially increases the rate of oxidation and precipitation of Fe(III)-bearing minerals in fractures (Jew et al., 2017). In this set of experiments, pyrite dissolution is observed to be rapid (i.e., non-detection by XRD after 30-days) which indicates the possibility of the above-

mentioned reaction processes which release iron and sulfides into solution for subsequent oxidation. These reactions are detrimental to reservoir permeability.

5.2.2 Iron Mineral Scale Formation

Iron mineral scale results from oxidation of Fe (II) released into solution following the breakdown of pyrite and other iron-based minerals. Fe-bearing minerals are generally present in almost all unconventional shale formations. During hydraulic fracturing, especially at the initial stages where acid fluids are injected, iron-bearing minerals are rapidly broken down. These minerals release Fe (II) into solution. Subsequent fluids with elevated levels of oxygen then cause the oxidation of Fe (II) into Fe(III). Most Fe (III) scales form within the rock matrix and may extend to the fracture face via micro fractures (Jew et al., 2022). This essentially blocks the permeability between the shale matrix and fracture network. Trends described above can be inferred from the results of experiments conducted in this study, therefore there is high probability of Fe-bearing mineral scale formation in the Caney Shale. Further and more conclusive data set would come from the core flooding experiments at reservoir temperature and pressure.

5.2.3 Barite Mineral Scale Precipitation

Barite precipitation is one of the serious formation damage mechanisms in hydraulically fractured reservoirs. This problem results from the mineralogical composition of shale rock formations, the chemical compositions of water used for hydraulic fracturing as well as the barium added as barite to drilling fluids. Elevated concentrations of sulfate and high total dissolved solids in water used for hydraulic fracturing has been identified as responsible for high barite precipitation in Marcellus Shale (Wilson and Van Briesen, 2013). Barite precipitation has also been identified as a common occurrence in the high carbonate Eagle Ford shale, where its formation has been detected to a depth of millimeters from fracture surfaces (Li et al., 2019). More problematic is the fact that barite precipitation has been observed where different types of treatment waters are used, including spring water, synthetic brine, lake water and simulated hydraulic fracturing fluid (Marcon et al., 2017; Paukert-Vankeuren et al., 2017: Dieterich et al., 2016). Studies on the critical factors controlling barite precipitation showed that presence of oxidants and the rate of sulfate dissolution into solution as crucial (Li et al., 2021). Furthermore, a major part of barite precipitation takes place during injection phase of hydraulic fracturing (Xiong et al., 2020). Barite precipitation in unconventional reservoirs essentially blocks formation permeability and renders hydrocarbons trapped following stimulation. The trends in barium concentrations as observed in the reacted fluid analyses show significant barium available to form barite in the presence of sulfate.

5.2.4 Strontium Mineral Scale Precipitation

Formations formed in inland sea environments have high strontium concentrations in their rock minerals due to the presence of strontium-bearing carbonates and sulfates (Kuznetsov et al., 2012; Walderhaug and Bjørkum, 1992). Dissolution and precipitation of these minerals, for example celestite ($SrSO_4$) has been witnessed for reservoirs with higher strontium mineral concentration

(Esteves et al., 2021; Esteves et al., 2022; Spielman-Sun et al., 2021) In addition, strontium adsorbed on clay minerals in shale leach out during hydraulic fracturing (Jew et al., 2020) This happens when fresh water is used as base fluid for hydraulic fracturing fluid and thus a chemical disequilibrium is created that needs re-equilibrating. In other instances, where brine with high concentration of strontium is used as base fluid for fracturing fluids, an encounter with carbonates and chlorides in the formation may cause precipitation of strontianite and celestite. This has been reported in Marcellus shale (Jew et al., 2022). Strontium concentrations observed in fluids in this study are sufficient to cause the precipitation of minerals mentioned above.

5.2.5 Other Potential Scale Minerals Precipitation in Caney Shale

Upon hydraulic fracturing, when rock formation minerals start to dissolve, the ionic concentrations of pore fluids increase. These concentrations reach critical limits and anions and cations in solution begin to react to form new minerals that precipitate. Studies have shown that barium outcompetes other alkaline earth elements to combine with sulfate precipitating as barite. Excess sulfate ions in solution will proceed to pair with calcium cations to form gypsum or anhydrite (Dieterich et al., 2016; Paukert-Vankeuren et al., 2017). The minerals precipitated are known to form scales on the walls of fractures and thus cause reduction in porosity and permeability of the rock formation matrix, which provides fluid flow to micro fractures, that feed into macro/meso fractures which connected to vertical hydraulic fractures connected to the wellbore.

6.0 Conclusions

Following from the results observed in this study and the discussions of these results in relation to published literature, the following conclusions are drawn:

- The presence of oxygen in fracturing fluids injected into the subsurface is a major precursor to reactions between fluid and formation. The influence of oxygenated fluid is observed in the total dissolution and oxidation of pyrite in the samples mostly within the first 7-days of reaction.
- The breakdown of pyrite and subsequent oxidation of sulfide to sulfate upon exposure to oxygenated fracturing fluid causes increased localized acidity that catalyzes the dissolution of carbonates and other minerals.
- The mineralogical transitions and concentrations of elements such as barium, strontium, iron etc. in reacted fluid indicates the Caney Shale is susceptible to the scale formation and precipitation of minerals detrimental to permeability of reservoir following hydraulic fracturing.
- The increase in weight percent of illite after reaction suggests precipitation of illite due to reactions between rock and fracturing fluid. Though these changes may be the result of renormalization of weight percent of minerals in the sample following dissolution of pyrite, dolomite and feldspars, the precipitation of illite remains plausible. The implication of this

change is that a relatively brittle fracture wall becomes relatively ductile, due to increased illite (clay) content, thus facilitating fracture closure.

- Increased amounts of amorphous phases are observed after 7-days of reaction, mainly within the clay zones of XRD diffractograms, which is interpreted as possible deflocculation and dispersal of clay minerals. This implies the potential of fines generation during rock interaction with hydraulic fracturing fluids. Fines migration has been established as a significant cause of formation damage in most clay-rich unconventional reservoirs in North America.

Acknowledgements

The authors would like to acknowledge the funding by DOE Award DE-FE0031776 from the U.S. Department of Energy, Office of Fossil Energy together with industry partner, through the National Energy Technology Laboratory. The authors wish to acknowledge Dr Fengyang Xiong and Loic Bethel Dje of the Hydraulic Barrier and Materials Characterization Laboratory at Oklahoma State University.

References

Abbasi, S., and Khamehchi, E. (2021). Investigation of permeability decline due to coupled precipitation/dissolution mechanism in carbonate rocks during low salinity co-water injection. *Energy Reports*, *7*, 125–135.

Alalli, A., Li, Q., Jew, A., Kohli, A., Bargar, J., Zoback, M., Kovscek, A. (2018). Effects of hydraulic fracturing fluid chemistry on shale matrix permeability. *SPE/AAPG/SEG Unconventional Resources Technology Conference*.

Amirthan, T., and Perera, M. S. A. (2023). Underground hydrogen storage in Australia: a review on the feasibility of geological sites. *International Journal of Hydrogen Energy*, *48*(11), 4300–4328.

Appelo, C. A. J., and Postma, D. (2005). *Geochemistry, groundwater and pollution: Leiden, The Netherlands*. AA Balkema Publishers.

Arnorsson, S., and Stefansson, A. (1999). Assessment of feldspar solubility constants in water in the range of 0 degrees to 350 degrees C at vapor saturation pressures. *American Journal of Science, 299*(3), 173–209.

Aslannezhad, M., Ali, M., Kalantariasl, A., Sayyafzadeh, M., You, Z., Iglauer, S., Keshavarz, A. (2023). A review of hydrogen/rock/brine interaction: Implications for Hydrogen Geo-storage. *Progress in Energy and Combustion Science*, *95*, 101066.

Awejori, G. A., Dong, W., Doughty, C., Spycher, N., Radonjic, M. (2024). Mineral and fluid transformation of hydraulically fractured shale: case study of Caney Shale in Southern Oklahoma. Geomechanics and Geophysics for Geo-Energy and Geo-Resources, 10(1), 128.

Awejori, G. A., Doughty, C., Xiong, F., Paronish, T., Spycher, N., Radonjic, M. (2022). Integrated Experimental and Modelling Study of Geochemical Reactions of Simple Fracturing Fluids with Caney Shale. *Energy & Fuels*, *36*(17), 10064–10081.

Berger, G., Lacharpagne, J. C., Velde, B., Beaufort, D., Lanson, B. (1997). Kinetic constraints on illitization reactions and the effects of organic diagenesis in sandstone/shale sequences. *Applied Geochemistry*, *12*(1), 23–35.

Blanc, P., Lassin, A., Piantone, P., Azaroual, M., Jacquemet, N., Fabbri, A., Gaucher, E. C. (2012). Thermoddem: A geochemical database focused on low temperature water/rock interactions and waste materials. *Applied Geochemistry*, *27*(10), 2107–2116.

Bratcher, J. C., Kaszuba, J. P., Herz-Thyhsen, R. J., Dewey, J. C. (2021). Ionic Strength and PH Effects on Water-Rock Interaction in an Unconventional Siliceous Reservoir: On the Use of Formation Water in Hydraulic Fracturing. *Energy Fuels*, *35*, 18414.

Credoz, A., Bildstein, O., Jullien, M., Raynal, J., Trotignon, L., Pokrovsky, O. (2011). Mixed-layer illite–smectite reactivity in acidified solutions: Implications for clayey caprock stability in CO2 geological storage. *Applied Clay Science*, *53*(3), 402–408.

Das, D., Mishra, B., Gupta, N. (2021). Understanding the influence of petrographic parameters on strength of differently sized shale specimens using XRD and SEM. *International Journal of Mining Science and Technology*, *31*(5), 953–961.

De Farias Esteves, B., Li, Q., Spielman-Sun, E., Jew, A., Bargar, J., Druhan, J. (2021). A reactive transport model for celestite precipitation in shale reservoirs subject to hydraulic fracturing. *AGU Fall Meeting Abstracts*, *2021*, H55B-0757.

Dieterich, M., Kutchko, B., Goodman, A. (2016). Characterization of Marcellus Shale and Huntersville Chert before and after exposure to hydraulic fracturing fluid via feature relocation using field-emission scanning electron microscopy. *Fuel*, *182*, 227–235.

Du, H. (2019). *Experimental Evaluation of How Mineralogy and Microstructure Impact Micro-Geomechanics of Shale Rocks*. Louisiana State University and Agricultural & Mechanical College.

Edgin, M. G., Medina-Rodriguez, B., Kaszuba, J. P., Dewey, J. C., Alvarado, V. (2021). Geochemical reactions and alteration of pore architecture in saturated shale after injection of stimulation fluid. *Fuel*, *303*, 120815.

Esteves, B. F., Spielman-Sun, E., Li, Q., Jew, A. D., Bargar, J. R., Druhan, J. L. (2022). Geochemical Modelling of Celestite (SrSO4) Precipitation and Reactive Transport in Shales. *Environmental Science & Technology*, *56*(7), 4336–4344.

Fakcharoenphol, P., Charoenwongsa, S., Kazemi, H., Wu, Y. S. (2013). The effect of water-induced stress to enhance hydrocarbon recovery in shale reservoirs. *SPE Journal*, *18*(05), 897–909.

Fritz, R. D., Medlock, P., Kuykendall, M. J., and Wilson, J. L. (2012). *The geology of the Arbuckle Group in the midcontinent: Sequence stratigraphy, reservoir development, and the potential for hydrocarbon exploration*.

Grieser, B., Wheaton, B., Magness, B., Blauch, M., Loghry, R. (2007). Surface reactive fluid's effect on shale. *SPE Oklahoma City Oil and Gas Symposium/Production and Operations Symposium*, SPE-106815.

Gundogar, A. S., Ross, C. M., Jew, A. D., Bargar, J. R., Kovscek, A. R. (2021). Multiphysics investigation of geochemical alterations in Marcellus shale using reactive core-floods. *Energy & Fuels*, *35*(13), 10733–10745.

Guo, Z. Q., Liu, C., Liu, X. W., Dong, N., Liu, Y. W. (2016). Research on anisotropy of shale oil reservoir based on rock physics model. *Applied Geophysics*, *13*(2), 382–392.

Güven, N., Lafon, G. M., Lee, L. J. (1982). *Experimental hydrothermal alteration of albite to clays: preliminary results*.

Harrison, A. L., Jew, A. D., Dustin, M. K., Thomas, D. L., Joe-Wong, C. M., Bargar, J. R., Johnson, N., Brown, G. E., Maher, K. (2017). Element Release and Reaction-Induced Porosity Alteration during Shale-Hydraulic Fracturing Fluid Interactions. *Appl. Geochem.*, *82*, 47.

Heidari, P., Li, L., Jin, L., Williams, J. Z., Brantley, S. L. (2017). A reactive transport model for Marcellus shale weathering. *Geochimica et Cosmochimica Acta*, *217*, 421–440.

Herz-Thyhsen, R. J., Kaszuba, J. P., Dewey, J. C. (2019). Dissolution of minerals and precipitation of an aluminosilicate phase during experimentally simulated hydraulic fracturing of a mudstone and a tight sandstone in the Powder River Basin, WY. *Energy & Fuels*, *33*(5), 3947–3956.

Holland, T. J. B., and Powell, R. (1998). An internally consistent thermodynamic data set for phases of petrological interest. *Journal of Metamorphic Geology*, *16*(3), 309–343.

Huang, W. L., Bishop, A. M., Brown, R. W. (1986). The effect of fluid/rock ratio on feldspar dissolution and illite formation under reservoir conditions. *Clay Minerals*, *21*(4), 585–601.

Isah, A., Arif, M., Hassan, A., Mahmoud, M., Iglauer, S. (2022). Fluid–rock interactions and its implications on EOR: Critical analysis, experimental techniques and knowledge gaps. *Energy Reports*, *8*, 6355–6395.

Jew, A. D., Bargar, J. R., Brownlow, J., Laughland, M. (2020). Strontium behavior in Midland Basin unconventional reservoirs: The importance of base fluids. *SPE/AAPG/SEG Unconventional Resources Technology Conference*.

Jew, A. D., Druhan, J. L., Ihme, M., Kovscek, A. R., Battiato, I., Kaszuba, J. P., Bargar, J. R., Brown Jr, G. E. (2022). Chemical and Reactive Transport Processes Associated with Hydraulic Fracturing of Unconventional Oil/Gas Shales. *Chemical Reviews*, *122*(9), 9198–9263.

Jew, A. D., Dustin, M. K., Harrison, A. L., Joe-Wong, C. M., Thomas, D. L., Maher, K., Brown Jr, G. E., Bargar, J. R. (2017). Impact of organics and carbonates on the oxidation and precipitation of iron during hydraulic fracturing of shale. *Energy & Fuels*, *31*(4), 3643–3658.

Josephs, R. E., Porlles, J., Tomomewo, O. S., Gyimah, E., Ebere, F. (2023). Geo-mechanical characterization of a well to store hydrogen. *ARMA US Rock Mechanics/Geomechanics Symposium*, ARMA-2023.

Katende, A., Allen, C., Rutqvist, J., Nakagawa, S., Radonjic, M. (2023). Experimental and numerical investigation of proppant embedment and conductivity reduction within a fracture in the Caney Shale, Southern Oklahoma, USA. *Fuel*, *341*, 127571.

Kuznetsov, A. B., Semikhatov, M. A., Gorokhov, I. M. (2012). The Sr isotope composition of the world ocean, marginal and inland seas: Implications for the Sr isotope stratigraphy. *Stratigraphy and Geological Correlation*, *20*, 501–515.

Lázaro, V. V. (2007). Illitization processes: Series of dioctahedral clays and mechanisms of formation. *Diagenesis and Low-Temperature Metamorphism. Theory, Methods and Regional Aspects; Nieto, F., Jiménez-Millán, J., Eds*, 31–39.

Li, Q., Jew, A. D., Cercone, D., Bargar, J. R., Brown Jr, G. E., Maher, K. (2019). Geochemical modelling of iron (hydr) oxide scale formation during hydraulic fracturing operations. *Unconventional Resources Technology Conference, Denver, Colorado, 22-24 July 2019*, 3863–3876.

Li, Q., Jew, A. D., Kohli, A., Maher, K., Brown Jr, G. E., Bargar, J. R. (2019). Thicknesses of chemically altered zones in shale matrices resulting from interactions with hydraulic fracturing fluid. *Energy & Fuels*, *33*(8), 6878–6889.

Li, Q., Wang, L., Perzan, Z., Caers, J., Brown Jr, G. E., Bargar, J. R., Maher, K. (2021). Global Sensitivity Analysis of a Reactive Transport Model for Mineral Scale Formation During Hydraulic Fracturing. *Environmental Engineering Science*, *38*(3), 192–207.

Lu, C., Zeng, Q., Liu, J., Ma, Z., Shao, X., Tang, L., Huang, Y., Zhou, G., Meng, X., Wang, J. (2023). Proppant embedment in rough fractures considering shale hydration. *Energy Reports*, *9*, 5146–5154.

Ma, L., Fauchille, A.L., Dowey, P. J., Figueroa Pilz, F., Courtois, L., Taylor, K. G., Lee, P. D. (2017). Correlative multi-scale imaging of shales: a review and future perspectives. *Geological Society, London, Special Publications*, *454*(1), 175–199.

Marcon, V., Joseph, C., Carter, K. E., Hedges, S. W., Lopano, C. L., Guthrie, G. D., Hakala, J. A. (2017). Experimental insights into geochemical changes in hydraulically fractured Marcellus Shale. *Applied Geochemistry*, *76*, 36–50.

Mukhina, E., Cheremisin, A., Khakimova, L., Garipova, A., Dvoretskaya, E., Zvada, M., Kalacheva, D., Prochukhan, K., Kasyanenko, A., Cheremisin, A. (2021). Enhanced oil recovery method selection for shale oil based on numerical simulations. *ACS Omega*, *6*(37), 23731–23741.

Ohazuruike, L., and Lee, K. J. (2023). A comprehensive review on clay swelling and illitization of smectite in natural subsurface formations and engineered barrier systems. *Nuclear Engineering and Technology*.

Olabode, A. O. (2012). *Experimental Investigations in CO 2 Sequestration and Shale Caprock Integrity*. Louisiana State University and Agricultural & Mechanical College.

Olabode, A., and Radonjic, M. (2017). Geochemical markers in shale-CO2 experiment at core scale. *Energy Procedia*, *114*, 3840–3854.

Osselin, F., Saad, S., Nightingale, M., Hearn, G., Desaulty, A. M., Gaucher, E. C., Clarkson, C. R., Kloppmann, W., Mayer, B. (2019). Geochemical and sulfate isotopic evolution of flowback and produced waters reveals water-rock interactions following hydraulic fracturing of a tight hydrocarbon reservoir. *Science of the Total Environment*, *687*, 1389–1400.

Paronish, T. J., Schmitt, R., Moore, J. E., Crandall, D., Rihn, A., Renk, J., Doughty, C., Bunger, A., Wang, Y., Katende, A. (2021). *Computed Tomography Scanning and Geophysical Measurements of the Caney Shale Formation from the Tomaney# 1-35-34-27 Well*. National Energy Technology Laboratory (NETL), Pittsburgh, PA, Morgantown, WV ….

Paukert Vankeuren, A. N., Hakala, J. A., Jarvis, K., Moore, J. E. (2017). Mineral reactions in shale gas reservoirs: barite scale formation from reusing produced water as hydraulic fracturing fluid. *Environmental Science & Technology*, *51*(16), 9391–9402.

Pruess, K., Oldenburg, C. M., Moridis, G. J. (1999). *TOUGH2 user's guide version 2*. Lawrence Berkeley National Lab (LBNL), Berkeley, CA (United States).

Radonjic, M., Luo, G., Wang, Y., Achang, M., Cains, J., Katende, A., Puckette, J., Grammer, M., King, G. E. (2020). Integrated microstructural characterisation of caney shale, OK. *Unconventional Resources Technology Conference, 20–22 July 2020*, 2157–2174.

Renock, D., Landis, J. D., Sharma, M. (2016). Reductive weathering of black shale and release of barium during hydraulic fracturing. *Applied Geochemistry*, *65*, 73–86.

Sonnenthal, E., Spycher, N., Xu, T., Zheng, L. (2021). *TOUGHREACT V4. 12-OMP and TReactMech V1. 0 Geochemical and Reactive-Transport User Guide*.

Spielman-Sun, E., Jew, A. D., Druhan, J. L., Bargar, J. R. (2021). Controlling strontium scaling in the Permian Basin through manipulation of base fluid chemistry and additives. *Unconventional Resources Technology Conference, 26–28 July 2021*, 1292–1301.

Swami, V., Clarkson, C. R., Settari, A. T. (2012). Non-Darcy flow in shale nanopores: do we have a final answer? *SPE Canadian Unconventional Resources Conference*.

Tarkowski, R., and Uliasz-Misiak, B. (2022). Towards underground hydrogen storage: A review of barriers. *Renewable and Sustainable Energy Reviews*, *162*, 112451.

Vidic, R. D., Brantley, S. L., Vandenbossche, J. M., Yoxtheimer, D., Abad, J. D. (2013). Impact of Shale Gas Development on Regional Water Quality. *Science*, *340*, 1235009.

Walderhaug, O., and Bjørkum, P. A. (1992). Effect of meteoric water flow on calcite cementation in the Middle Jurassic Oseberg Formation, well 30/3-2, Veslefrikk Field, Norwegian North Sea. *Marine and Petroleum Geology*, *9*(3), 308–318.

Wang, Y., Luo, G., Achang, M., Cains, J., Wethington, C., Katende, A., Grammer, G. M., Puckette, J., Pashin, J., Castagna, M. (2021). Multiscale characterization of the caney shale—an emerging play in Oklahoma. *Midcontinent Geoscience*, *2*, 33–53.

Wilson, J. M., and Van Briesen, J. M. (2013). Source water changes and energy extraction activities in the Monongahela River, 2009–2012. *Environmental Science & Technology*, *47*(21), 12575–12582.

Xiong, F., Rother, G., Radonjic, M. (2022). Insights into Controls of Mineralogy and Pore Structure on the Density of Methane Adsorption Phase in Shales under Supercritical Conditions. *Energy & Fuels*, *36*(17), 10110–10122.

Xiong, W., Lopano, C., Hakala, A., Carney, B. J. (2020). Investigation of barite scaling during reaction between pre-treated hydraulic fracturing fluid from the field and Marcellus Shale. *SPE/AAPG/SEG Unconventional Resources Technology Conference*.

Xu, T., Spycher, N., Sonnenthal, E., Zhang, G., Zheng, L., Pruess, K. (2011). TOUGHREACT Version 2.0: A simulator for subsurface reactive transport under non-isothermal multiphase flow conditions. *Computers & Geosciences*, *37*(6), 763–774.